

THE ROLE OF MULTIPLE-VORTEX TORNADO STRUCTURE IN CAUSING STORM RESEARCHER FATALITIES

BY JOSHUA WURMAN, KAREN KOSIBA, PAUL ROBINSON, AND TIM MARSHALL

An extremely large and powerful Doppler On Wheels–observed tornado, with several embedded intense multiple-vortices, moving rapidly in complex troichoid-like paths, killed and injured several storm chasers.

Researchers, recreational storm chasers, storm-chasing tours, storm spotters, television reporters, and others have been pursuing tornadic storms for centuries to satisfy a variety of goals. As early as 1755, Benjamin Franklin describes a tornado chase on horseback (van Doren 1938). Until recently, within the storm-chasing and research community, there have been no known fatalities or significant injuries directly caused by tornadoes.

Attempts to deploy instrumentation in the path of tornadoes have been made since the 1970s in order to map the wind field and other properties of tornadoes (Bluestein and Bedard 1982; Brock et al. 1987; Tatom and Knupp 1995; Bluestein 1999; Winn et al. 1999; Lee et al. 2004; Samaras 2004; Wurman and Samaras 2004;

Karstens et al. 2010; Lee et al. 2011). An armored vehicle has collected data inside tornadoes in conjunction with radar observations (Wurman et al. 2007b, 2013). Data have been collected by vehicles accidentally penetrating tornadoes (Kosiba and Wurman 2013). Mobile radars, such as the Doppler on Wheels (DOW) and the Rapid-Scan DOW (RSDOW) (Wurman et al. 1996, 1997, 2013; Wurman 2002, 2008; Wurman and Gill 2000; Wurman 2002; Lee and Wurman 2005; Kosiba et al. 2008; Kosiba and Wurman 2010; Wakimoto et al. 2012; Wurman and Kosiba 2013, hereafter WK13) and others (Bluestein et al. 1997, 2003, 2004; Bluestein and Pazmany 2000, Tanamachi et al. 2007) have deployed near tornadoes since the 1990s to map the three-dimensional fields of wind, precipitation, and debris.

Those pursuing storms typically are highly mobile and well aware of the associated hazards. The highest-impact portions of tornadoes are relatively small¹ and short lived; thus, the risks posed to storm chasers by tornadoes are relatively minor. Although the region containing potentially marginally damaging ground-relative winds $V_g > 30\text{--}40\text{ m s}^{-1}$ occasionally has a diameter of $>4\text{ km}$ (Wurman 2002; WK13), these

AFFILIATIONS: WURMAN, KOSIBA, AND ROBINSON—Center for Severe Weather Research, Boulder, Colorado; MARSHALL—Haag Engineering, Irving, Texas

CORRESPONDING AUTHOR: Joshua Wurman, Center for Severe Weather Research, 1945 Vassar Circle, Boulder, CO 80305
E-mail: jwurman@cswr.org

The abstract for this article can be found in this issue, following the table of contents.

DOI:10.1175/BAMS-D-13-00221.1

In final form 16 September 2013
©2014 American Meteorological Society

¹ The average diameter of the region enclosing the most intense winds in a tornado is 300 m (Alexander and Wurman 2008), very rarely reaching $\sim 2\text{ km}$ in extremely large tornadoes/MVMCs (Wurman 2002; WK13).

wind intensities pose only low/moderate risks to those in vehicles. The life-threatening portion of a tornado is usually avoidable by chasers. The low success rate of intentional vehicular penetrations of tornadoes stands as evidence that it is difficult to even purposely penetrate the core flow region.

However, a team attempting to deploy instrumentation was killed on 31 May 2013 when their vehicle was impacted and thrown by a tornado southeast of El Reno, Oklahoma. A media team suffered major

vehicle damage and injuries when their vehicle was thrown.

THE EL RENO TORNADO. During the afternoon of 31 May 2013, a discontinuous line of thunderstorms formed in western Oklahoma, from near Weatherford, extending northeast. Shortly after a cell merger/interaction at the southern edge of this convection,² the first tornado warning was issued by the National Weather Service (NWS) at 2236 UTC

31 May 2013, and a tornado was reported at 2255 UTC (though the tornado track posted by the NWS begins at 2303 UTC) (www.srh.noaa.gov/oun). Based on NWS and DOW data, the tornado circulation grew in both size and intensity into a large tornado/multiple-vortex mesocyclone (MVMC) that tracked generally east-southeastward; then tracked eastward until 2318 UTC; crossed U.S. Highway 81 (US-81) near 2319 UTC south of El Reno, Oklahoma; then moved generally northeastward to Interstate 40 (I-40); became nearly stationary for several minutes, possibly looping on itself, before moving eastward along and near I-40; and then became nearly stationary or looping again near I-40, as it dissipated at 2345 UTC³ (Fig. 1).

Overview from the KTLX WSR-88D. The dual-polarization KTLX Weather Service Radar-1988 Doppler (WSR-88D) observed a strong vortex signature after 2305 UTC from a range of about 75 km (Fig. 2). At this time, gate-to-gate

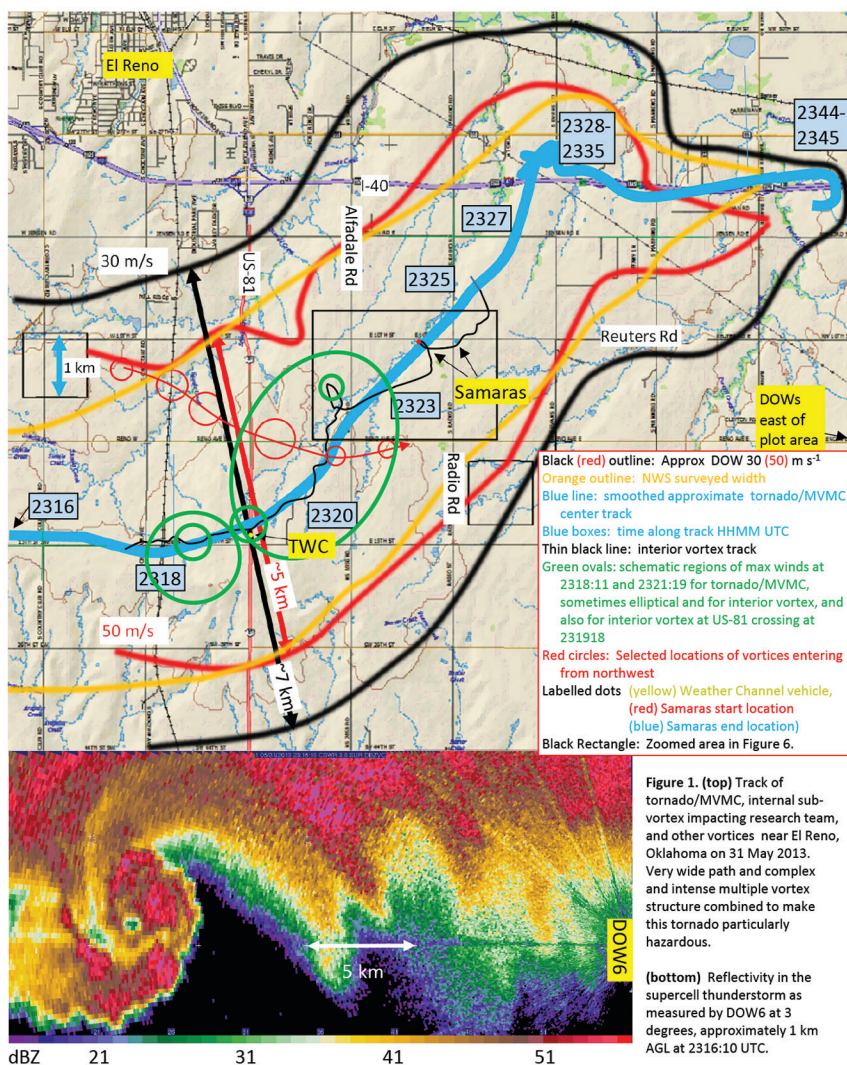


FIG. 1. (top) Track of tornado/MVMC, internal subvortex impacting research team, and other vortices near El Reno, Oklahoma, on 31 May 2013. The very wide path and complex and intense multiple-vortex structure combined to make this tornado particularly hazardous. **(bottom)** Reflectivity in the supercell thunderstorm as measured by DOW6 at 3°, approximately 1-km AGL at 2316:10 UTC.

² The mechanism of tornadogenesis is beyond the scope of this paper. The role of mergers in tornadogenesis has been explored elsewhere: for example, Wurman et al. (2007a) and Hastings et al. (2012a,b).

³ Dissipation time based on DOW observations.

shear exceeded 50 m s^{-1} and there was a suggestion of a developing but barely resolvable low reflectivity eye (LRE) but no prominent debris signature (DS) in either the differential reflectivity (ZDR) or ρ_{HV} fields. By 2314 UTC, the circulation had grown and intensified. There is a suggestion (confirmed using finescale-resolution DOW data) of quasi-concentric wind field maxima, one with a diameter, from peak inbound to peak outbound Doppler velocity, $\text{DX}_{\text{max}} = 1\text{--}2 \text{ km}$ and the other much smaller. However, at $\sim 60\text{-km}$ range, the KTLX radar has a beamwidth of $>1 \text{ km}$ and does not resolve sub-kilometer-scale features. Both ZDR and ρ_{HV} fields reveal lower values in the region of most intense winds, likely caused by lofted debris (Ryzhkov et al. 2005; Bluestein et al. 2007). A prominent region of high ZDR ($>2 \text{ dB}$), moderate reflectivity ($>45 \text{ dBZ}$), and high ρ_{HV} (>0.9) wraps around the circulation and also protrudes slightly southwestward. This signature extends north and then east-southeastward along the edge of the supercell coincident with a region of inferred inflow, similar to the observations

of Kumijan (2011), who suggests that this is indicative of large drops able to fall out of the periphery of the updraft (while smaller drops are carried aloft). Low ZDR ($<1.0 \text{ dBZ}$) and high ρ_{HV} on the west side of the hook is suggestive of small drops, possibly forced downward within the rear-flank downdraft (Kumijan 2011). By 2319 UTC, the large tornado/MVMC circulation had grown and intensified further with two prominent shear/rotation signatures evident to the east and west of the center of circulation. The

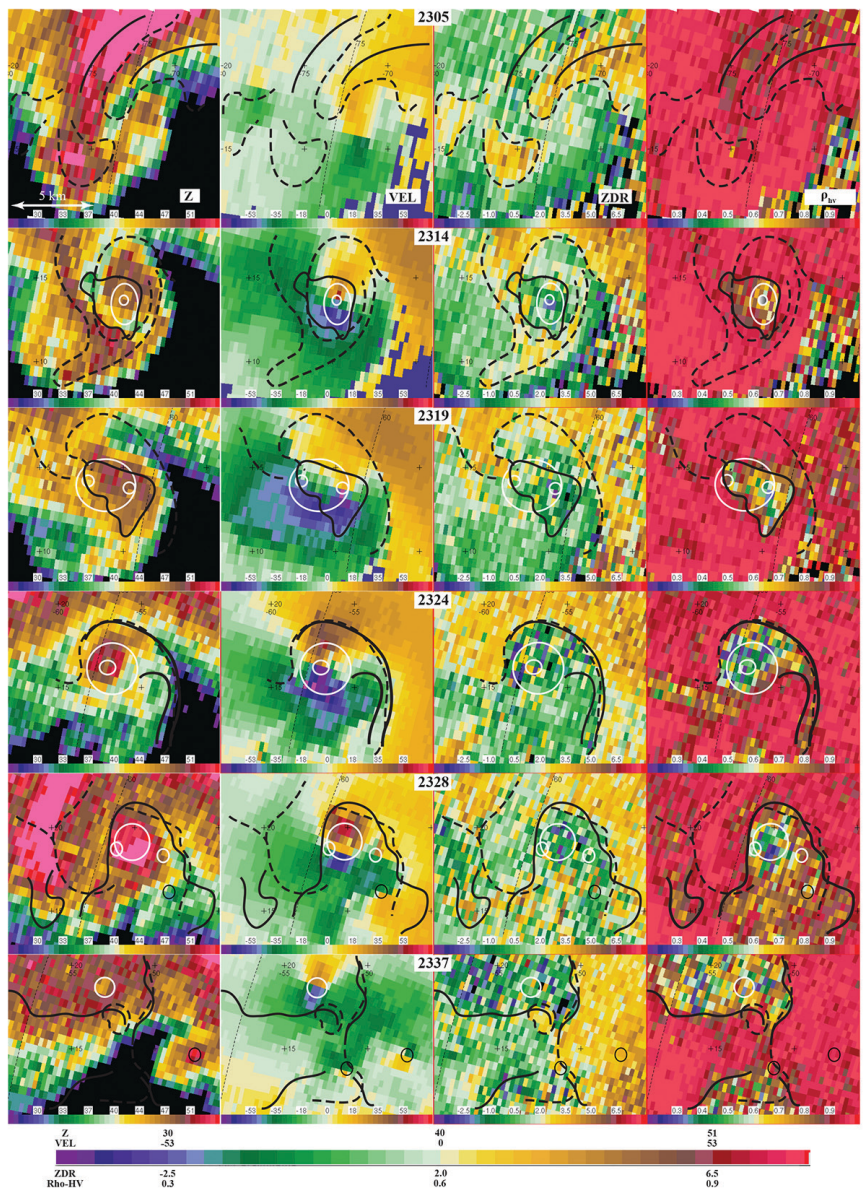


FIG. 2. El Reno tornado and anticyclonic tornado as observed by KTLX: (left)–(right) reflectivity, Doppler velocity, differential reflectivity, and the cross-correlation coefficient. Prominent vortices, including the large tornado/MVMC and visible internal vortices, are outlined in white. Anticyclonic vortices (one of which is a tornado) are in outlined in black. Stippled (solid) black lines indicate interesting regions of high (low) ZDR (ρ_{HV}) fields.

stronger eastern circulation was associated with a barely discernible LRE, while none is visible to the west. Both vortices are located in a region of low ρ_{HV} and low ZDR, but values are lower near the eastern one, likely because the eastern vortex/shear zone is more intense, thus lofting more debris. By 2324 UTC, a LRE is more distinct and surrounded by a debris ring echo (DRE) (low ρ_{HV} and low ZDR), which is approximately collocated with an inner vortex. A large region of low ZDR and ρ_{HV} extends for 3–5 km near

the circulation center, indicative of continued—and perhaps more extensive—debris lofting. To the immediate east of the circulation, an arc of low ρ_{HV} connects to the near-circulation region of low ρ_{HV} . This arc of low ρ_{HV} is coincident with a large gradient in reflectivity and Doppler velocity along the knob of the hook. The tornado signature weakens by 2333 UTC (not shown) and then reintensifies by 2338 UTC but not to its earlier strength before finally dissipating. At 2333 and 2338 UTC an anticyclonic wind couplet is evident several kilometers to the southeast of the primary tornado. At 2338 UTC two such circulations can be seen, but DOW data (discussed below) reveal that only one of these KTLX-observed vortices at ~ 1 km AGL is manifested as a tornado near the surface (~ 100 m AGL).

DOW dual-polarimetric observations of the tornado.

Two DOWs deployed in the path of the supercell after 2316 UTC (Wurman et al. 1997; Wurman 2001). The dual-polarization, dual-frequency DOW6 radar collected data in the tornado from 2316 to 2323 UTC at 35.4415°N, 97.7244°W and from 2335 to 2341 UTC at 35.4788°N, 97.7775°W (between, before, and after these times DOW6 scanned during very short deployments and while mobile), and the RSDOW deployed from 2318 to 2327 UTC at 35.4348°N, 97.7776°W and from 2329 to 2348 UTC at 35.4376°N, 97.7775°W, both documenting evolution of the most intense, complex, and largest phases of the tornado.⁴

The DOW radars, deployed at $\frac{1}{4}$ the range of KTLX, 12–15 km from the tornado in most data presented here, with low-level updates at 15–43 times shorter intervals, allowed for the exploration of the structure and evolution of the tornado/MVMC and its internal subvortices at much finer temporal and spatial scale. At 2316 UTC, DOW6 revealed structures in the tornado/MVMC similar to but in finer detail than those observed by KTLX at 2315 UTC, such as an LRE coincident with values of slightly reduced ρ_{HV} and low ZDR (Fig. 3).⁵ The arc of high ZDR and region of low ZDR also are evident. Despite wavelength differences and differences in observation geometry, the X-band (3-cm radiation) DOW6 and S-band (10-cm radiation) KTLX ZDR and ρ_{HV} fields are consistent, particularly when compared for similar times (e.g., 2319 and 2324 UTC), providing confidence in the DOW mapping of small-scale features invisible to

KTLX. The better resolution of the DOW6 data reveals that, at 2316 UTC, a region of large velocities is coincident with a region of lower ZDR along the west side of the hook, perhaps suggesting an enhanced region of downward motion, as discussed above. At 2319 UTC DOW data reveal that the high ZDR spiral, though still wrapping around to the east side of the tornado, has become diffuse; a weakened LRE persists; and two vortices exhibiting lower ZDR and moderate ρ_{HV} are present well to the northwest of the main tornado. DOW6 data at 2323 UTC show that the arc of high ZDR, while still wrapping into the knob of the hook, is less distinct. The central low ρ_{HV} and ZDR regions are comma shaped, possibly as a result of debris and/or hail centrifuging (e.g., Dowell et al. 2005; Bluestein et al. 2007). At 2325 UTC, at 2 km AGL, there is a large region of low ZDR well beyond the LRE and extending beyond the region of low ρ_{HV} . Within the low ρ_{HV} region there is a region exhibiting high ρ_{HV} values with only a slight increase in ZDR on the southwestern periphery. The high ρ_{HV} region overlaps the LRE and a region of high reflectivity to the south of the LRE (coincident with the slightly higher ZDR values). Based on the overlap of these fields, it is possible that smaller drops are present closer to the center of the circulation, while larger drops are present farther outward. Since these observations are from a height of approximately 2 km AGL, differential centrifuging and/or fallout may be possible. KTLX observations near this time do not resolve these finescale details.

Rapid-Scan DOW observations of the tornado. RSDOW data collection, commencing after 2317:30 UTC, permitted study of even finer spatial- and temporal-scale evolution of velocity structures and the resolution of rapid changes in reflectivity features identified using dual-polarization data from DOW6. The large circulation and the interior vortex move rapidly eastward, crossing US-81 at a speed, $V_p \sim 25$ m s⁻¹, comparable to the highest speeds ever documented by DOW radar observations, while the diameter of the interior subvortex increases from $DX_{\text{max}} = 150$ to 350 m. (This high V_p likely contributed to injuries among a media team, as discussed below.) At 2317:38–2318:48 UTC, two comparable intensity circulations are evident, one inside the other, with diameters between maximum inbound and outbound winds, $D \sim 2000$ and 150 m, similar

⁴ The RSDOW and DOW have 0.9° beam widths, sample at 50-m (RSDOW) and 30–60-m (DOW6) gate lengths, and scan at 50° s⁻¹ to produce volumetric updates at 7-s (RSDOW: 6 elevations) and 21-s (DOW6: 3 elevations) intervals.

⁵ The 3° elevation scans are used because of partial beam blockage below that level. The Rapid-Scan DOW deployed at a site with minimal blockage, so even 0.5° elevation scans are usable.

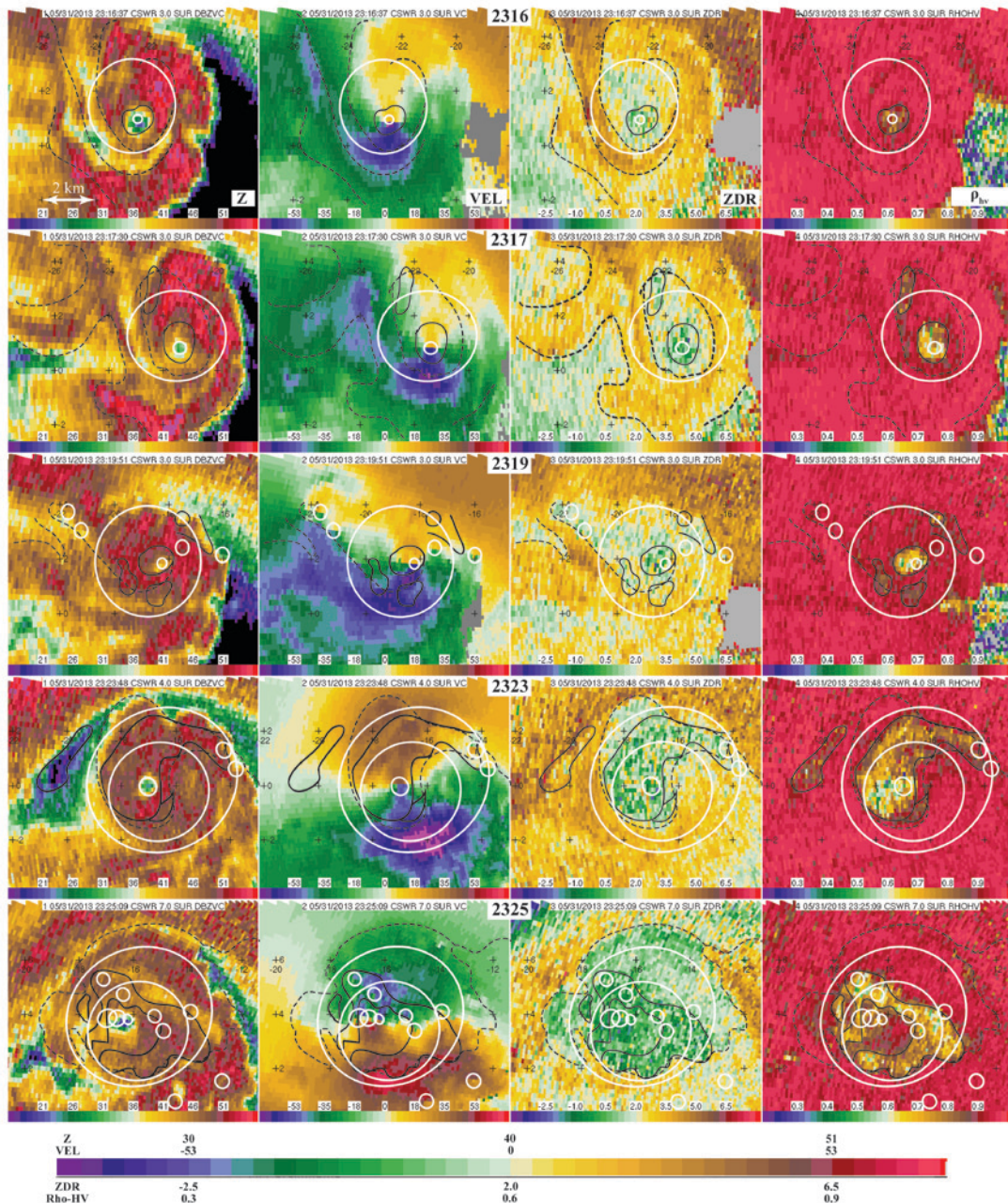


FIG. 3. El Reno tornado and anticyclonic tornado as observed by DOW6: (left)–(right) reflectivity, Doppler velocity, differential reflectivity, and the cross-correlation coefficient. Prominent vortices, including the large tornado/MVMC and visible internal vortices, are outlined in white. Stippled (solid) black lines indicate interesting regions of high (low) ZDR (ρ_{HV}) fields.

to structures observed before [e.g., Kellerville, Texas (1995), and Harper, Kansas (2004); WK13] (Fig. 4). The larger circulation is best described as a large tornado/

MVMC with a single (at this time) embedded subvortex following the nomenclature of WK13.⁶ Additional vortices, especially prominent from 2318:48 to 2321:19 UTC,

⁶ Alternately, the interior subvortex (subvortices) could be described as a distinct tornado (tornadoes) embedded in a mesocyclone. However, then the width of damage caused by each of these tornadoes (as opposed to damage caused by the mesocyclone) would be <1 km. Also, while one subvortex is persistent, others are transient, and sometimes up to several are observed simultaneously. So, if the subvortices are described as tornadoes, then it would follow that this event comprised several (at least) individual small to moderate sized tornadoes.

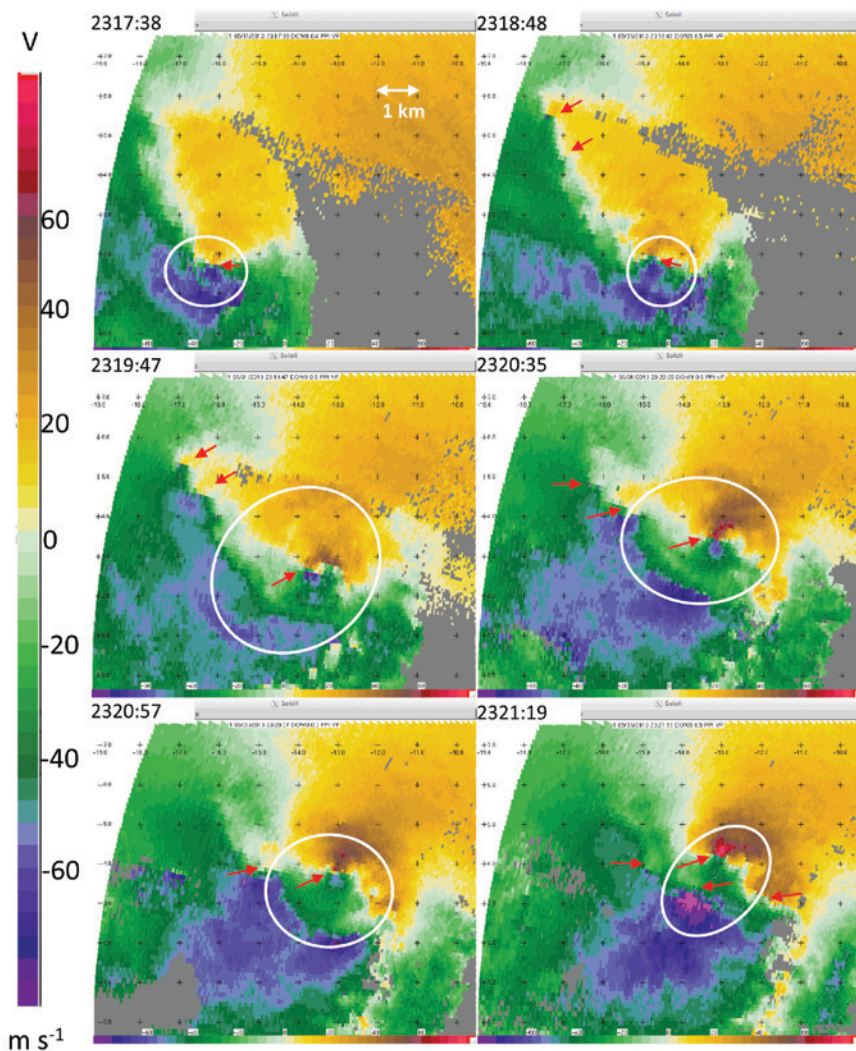


FIG. 4. Evolution of the tornado/MCMV from 2317:38 to 2321:19 UTC as observed by the RSDOW. White circles denote the larger-scale vortex and the red arrows denote subvortices. After 2318 UTC, the winds associated with the larger-scale vortex are comparable to or smaller than the interior subvortex. The region enclosing maximum winds of the MVMC is sometimes very elliptical.

external to the primary circulation move toward it from the northwest and are ingested in a pattern similar to that observed in the Seward, Kansas (2008), and Oklaunion, Texas (2000), tornadoes (WK13). While it is subjectively delineated, especially because of the perturbing effects of subvortices, the region enclosing the most intense winds in the larger tornado/MVMC is sometimes apparently quite elongated, sometimes obliquely to the track (e.g., at 2320:57 UTC) and at other times along the track (e.g., 2321:19 UTC).

be consistent with revolving about a larger vortex at a radius of 750–1000 m at a speed of $\sim 30\text{--}40\text{ m s}^{-1}$.

Doppler velocities $> 115\text{ m s}^{-1}$ are observed in the subvortex just after 2326 UTC while the vortex is moving at an appreciable angle across the RSDOW radar's beams. If axisymmetry and a simple Rankine-type profile are assumed and an assumed component of the very large but unobserved V_p of the subvortex is vectorially added (following Wurman et al. 2007b, where only $\sim 1\text{ m s}^{-1}$ was added), peak V_g in this vortex ranges

An important structural change occurs after 2320 UTC; the interior subvortex, which was nearly concentric with the larger tornado/MVMC and moving with a similar V_p , is displaced. Additional vortices are also more apparent. Some of these vortices are associated with individual LREs and DREs (Fig. 5f). The most intense vortex begins a trochoidal, sometimes prolate cycloidal,⁷ motion about the larger circulation (Fig. 6), possibly similar to what was observed by a DOW in the Geary, Oklahoma (2004) tornado/MVMC (WK13). The period between the apices of the retrograde loops at 2321:31 and 2323:46 UTC (and, by extrapolation, as the vortex becomes difficult to track at about 2326 UTC) was approximately 130 s. The subvortex becomes nearly stationary at the northwest extreme of the loops and moves at speeds of up to 79 m s^{-1} (the fastest ever documented) on the southeastern side of the larger tornado. Very approximately, these speeds and looping period would

⁷ True trochoids/cycloids are created by tracing lines created by points on nonslipping wheels. Most tornadoes, however, have peak tangential velocities $V_t > V_p$, analogous to slipping wheels. Since the structure of the large tornado/MVMC is evolving and the tornado is moving in curved path, possibly revolving about a larger circulation, the prolate cycloidal description of the path of the subvortex is qualitative.

FIG. 5. (left) Doppler velocity and (right) reflectivity. (top) Strong vortices and exterior vortex, with LRE and DS/DRE signatures (blue rings). (middle) Large along-track width of 30 and 50 m s⁻¹ radar winds, ~2-km diameter circulation, and strong interior vortex. The red oval delineates approximate region with inferred winds > 50 m s⁻¹. (bottom) Several subvortices. Blue rings schematically illustrate DREs. Black rings denote velocity signatures of subvortices.

from 130 to 150 m s⁻¹, which is comparable to the highest ever reported. However, three factors complicate this comparison: 1) the current measurements are ~100 m AGL, adding great uncertainty concerning how to reduce to near-ground levels (e.g., 10 m AGL); 2) there is uncertainty in the extremely high V_p of the subvortex and its angle relative to the DOW beams; and 3) the duration of the highest DOW-measured winds corresponds to <<1-s wind gusts over any fixed location (Fig. 7). Even if peak V_g (100 m AGL) = 140 m s⁻¹ in a small, extremely rapidly moving subvortex, a stationary observer/structure even at that height would only experience $V_g > 130$ m s⁻¹ for ~0.5 s, much less than the 3-s duration typically used when quantifying wind impacts. The 3-s average V_g caused by this subvortex would be <100 m s⁻¹, depending mostly on the

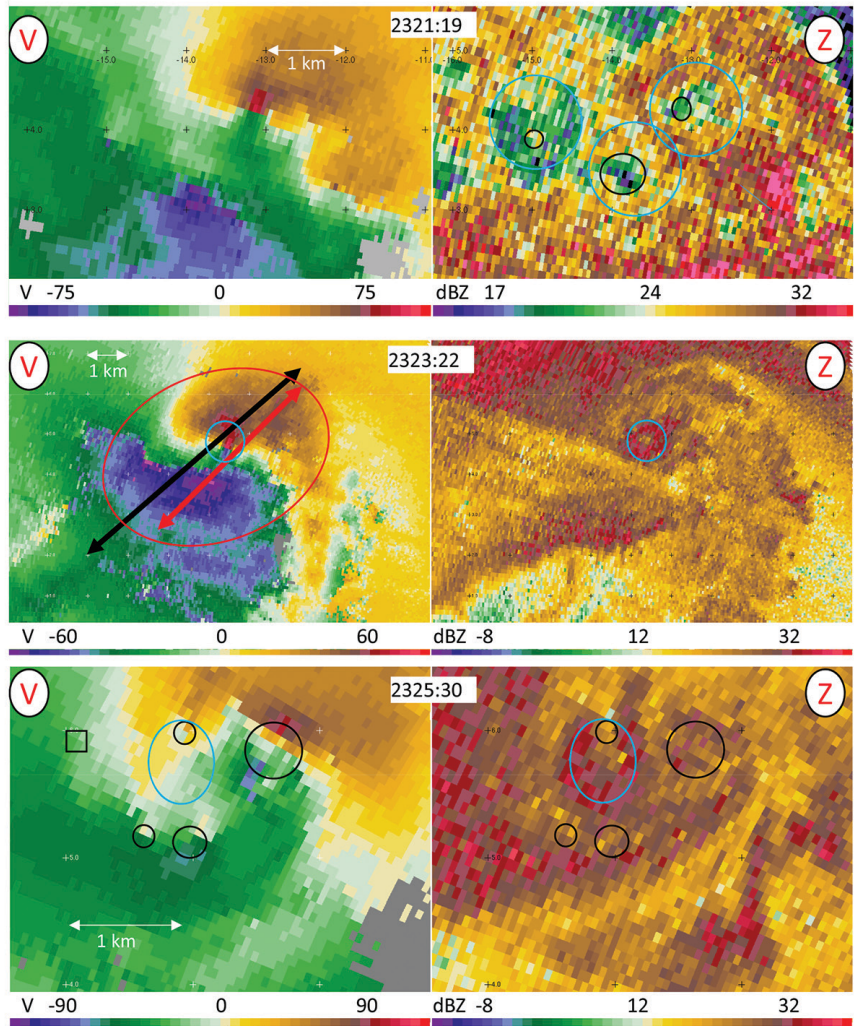
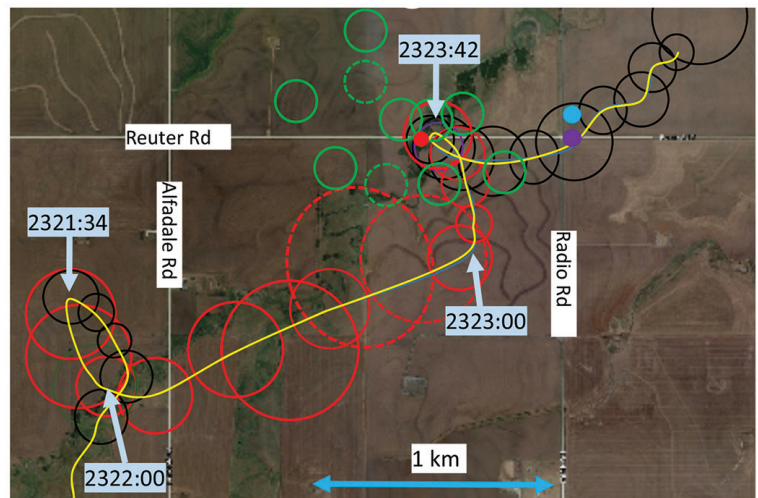


FIG. 6. Smoothed track of interior subvortex as measured by the Rapid-Scan DOW. The yellow line is the approximate center of circulation. Red and black circles delineate, at selected times, the approximate region enclosing the maximum tangential velocity V_{tm} . Blue boxes label selected times along the track in HHMM:SS UTC. Red (blue) (purple) dots represent start (end) (post-storm relocation) locations of the Samaras team's vehicle. Green circles delineate vortices impacting the same area shortly afterward. The vortex executes a loop at 2321:34 UTC; moves rapidly east-northeastward from 2322 to 2323 UTC then more slowly north-northwestward, becoming stationary over Reuters road and the vehicle; and then moves east-northeastward again.



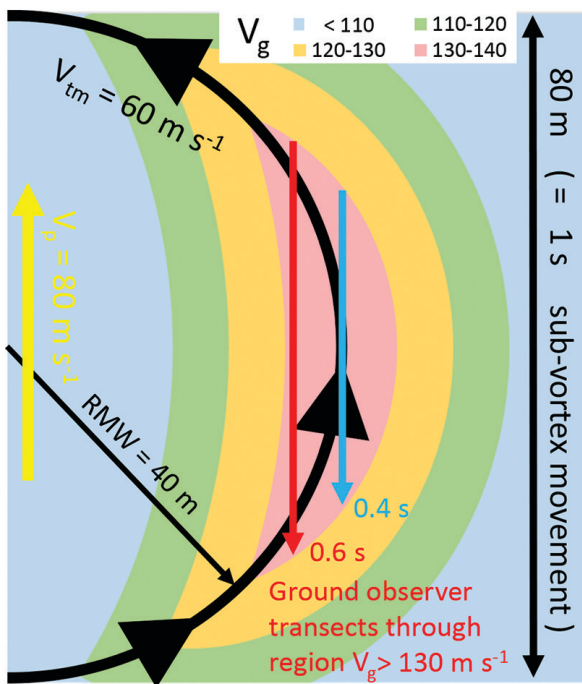


Fig. 7. Schematic of strong V_g side of rapidly moving subvortex: very fast $V_p = 80 \text{ m s}^{-1}$; adds to peak tangential winds $V_{tm} = 60 \text{ m s}^{-1}$; and at and near the radius of maximum winds resulting in peak $V_g = 140 \text{ m s}^{-1}$. However, due to very fast V_p , the duration of $V_g > 130 \text{ m s}^{-1}$ over a stationary object or observer is $\leq 0.6 \text{ s}$.

intensity of the surrounding flow, not the peak V_g in the subvortex.

The width of the MVMC, defined by a region enclosing DOW-measured $V_g > 30 \text{ m s}^{-1}$ (or alternatively 50 m s^{-1}), representing wind speeds potentially capable of causing marginal or substantial damage but excluding the large rear-flank downdraft to the south of the tornado DX_{30} (DX_{50}) increased rapidly from 1.4 km (0.6 km) at 2317 UTC to a maximum of 7 km (5 km) near 2319 UTC (Fig. 5), perhaps the widest ever documented.⁸ By comparison, Wurman (2002) reported $DX_{max} = 1.6 \text{ km}$ and $DX_{30} = 4.5 \text{ km}$ in the Mulhall, Oklahoma (1999), tornado and WK13 documented $DX_{max} \sim 2 \text{ km}$ in two tornadoes. Notably, however, dual-polarization evidence of debris from finescale DOW data below 1 km AGL is limited to a much smaller region, less than $2 \text{ km} \times 3 \text{ km}$ (Fig. 3), corresponding most closely to DX_{max} not DX_{50} , suggesting that substantial production and/

or lofting of debris is not occurring throughout the entire region enclosed by DX_{50} .

After 2325 UTC, the tornado/MVMC contracts and exhibits a multiple-vortex structure with several comparable intensity subvortices, more typical of Mulhall (1999) (Wurman 2002; Lee and Wurman 2005) (Fig. 5). While this is the first time that this particular evolution, from interior near-center subvortex to offset vortex to multiple comparable intensity vortices, has been documented, a range of MVMC evolutions have been observed previously: for example, in Quinter, Kansas (2008) (WK13), where a singlet tornado evolved into an MVMC, which then evolved back into a singlet tornado. The El Reno tornado moves northward, then becomes nearly stationary/looping near I-40 for $\sim 400 \text{ s}$ from 2328 to 2335 UTC, and then moves eastward for several minutes until becoming nearly stationary or looping again while dissipating at 2345 UTC, suggestive that the larger circulation is itself moving in a trochoidal fashion inside a larger mesocyclone.

In addition to the complex and changing structure of the main tornado/MVMC, the parent thunderstorm spawned a rare strong anticyclonic tornado with peak $V_g = 65 \text{ m s}^{-1}$ at $\sim 2328 \text{ UTC}$ in the anticyclonic shear zone to the southeast of the main tornado/MVMC, exhibiting multiple-vortex structure and a dual-polarimetric debris signature and lasting until $\sim 2343 \text{ UTC}$ (Fig. 8). The subvortices are associated with LREs and perturbations in the DS of the tornado in a sometimes-elliptical region exhibiting reduced ZDR and ρ_{HV} . To the authors' knowledge, this is the first ever time subvortices and DSs have been documented in an anticyclonic tornado. DOW data show that the second anticyclonic velocity couplet observed by both KTLX and DOWs did not extend to near the ground ($< 100 \text{ m AGL}$).

TORNADO IMPACTS STORM-CHASING TEAMS. The vehicle operated by Tim Samaras, his son Paul Samaras, and Carl Young was discovered at approximately 35.4795°N and 97.9014°W , about 50–100 m northeast of the intersection of Reuters Road/10th Street and Radio Road (Figs. 6, 9). The vehicle can be observed at 2122:15 in a video collected by a storm chaser (Dan Robinson) traveling east on Reuters Road, east of Alfadale Road. When impacted by the tornado, the vehicle was located approximately

⁸ Tornado width is poorly and subjectively defined. It is variously described as the distance across different Doppler velocity thresholds; the distance perpendicular to the track in which damage is documented; the maximum width, in any direction, of winds over a threshold; and the diameter of the core flow region. The DX_{50} in this tornado exceeds that observed by DOWs in any other tornado. Maximum DOW-measured cross-track width is observed earlier, at about 2318 UTC (Fig. 1). The extreme cross-track width of observed damage may have been enhanced by damage caused by external vortices.

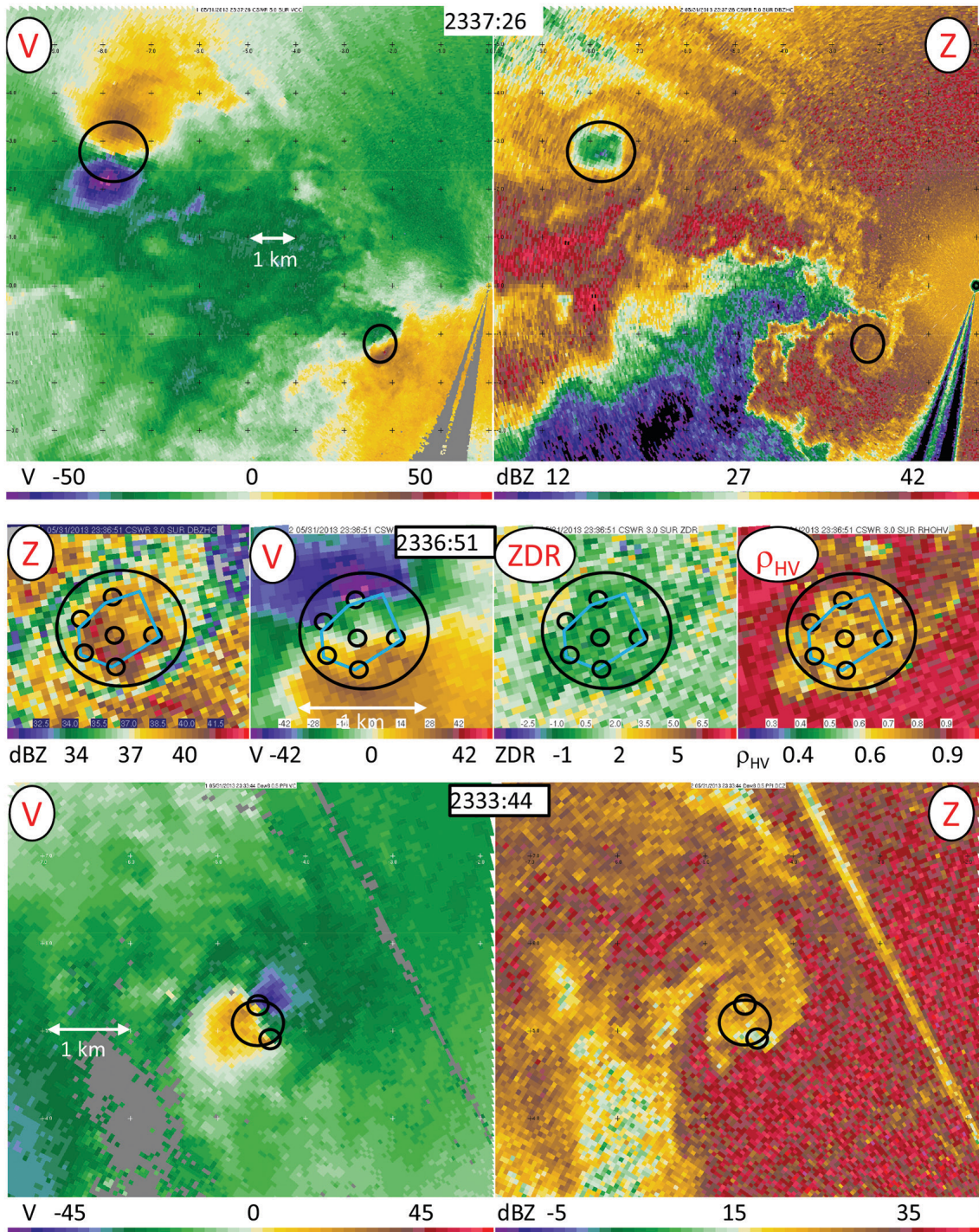


FIG. 8. (top) Anticyclonic tornado (left) Doppler velocity and (right) reflectivity in cyclonic and anticyclonic tornado. (middle) DOW6 reflectivity, velocity, ZDR, and ρ_{HV} . Blue polygon denotes quasi-polygonal DRE in region of reduced ZDR and ρ_{HV} . (bottom) Multiple-vortex structure of the anticyclonic tornado is evident in both RSDOW velocity and reflectivity fields.

530 m west of the intersection of Reuters and Radio Roads, near where Reuters Road crosses over an intermittent stream. The trunk contents were found just south of this location. Based on debris locations, the inferred path of the vehicle is southward,

eastward, and then east-northeastward to its resting place. The vehicle was destroyed and the researchers were killed (obituary: www.economist.com/news/obituary/21579436-tim-samaras-storm-chaser-and-researcher-died-may-31st-aged-55-tim-samaras).

Although the El Reno tornado was exceptional with respect to both size and intensity, Samaras had extensive experience deploying instrumentation in and near tornadoes, some of which were large, intense, and complex in structure (Lee et al. 2004, 2011; Wurman and Samaras 2004; Karstens et al. 2010). Since the members of this team died despite having experienced leadership, the circumstances leading to their deaths have particular importance to tornado researchers as well as recreational, media, and storm-tour chasers, whose missions bring them near tornadoes.



FIG. 9. (top) Tim Samaras's and (bottom) the Weather Channel's vehicles after they were transported by winds in the embedded subvortex inside the large tornado. Moderate damage to trees is evident. Samaras's vehicle was moved post-storm, before this photo.

It is likely that many details of the events leading to the deaths of the Samaras team will remain unknown. However, with the aid of DOW data and video documentation, it is possible to reconstruct some of the key details of the meteorological conditions leading to the destruction of their vehicle and speculate why this team fell victim. Visible in the video, the Samaras team drove eastward on Reuters Road and they penetrated the ~2-km-diameter core flow region of the large tornado/MVMC, just behind the Robinson vehicle, at about 2321–2322 UTC. Conditions at the north edge of and inside this circulation were quite harsh, as evident in the video, but not nearly as severe as on the south/strong side. The Robinson vehicle moved eastward at approximately 20 m s^{-1} , but the Samaras vehicle is seen to fall behind. One or more condensation funnels, likely associated with the DOW-observed subvortex, are visible to the south of the road. In the video, the Samaras vehicle's headlights are last seen to the west of Radio Road at 2322:15 UTC.

The above-described subvortex transcribes a loop: it becomes nearly stationary near 35.473°N , 97.923°W at 2321:31 UTC; then moves rapidly around the south side of the tornado with V_p averaging 25 m s^{-1} , peaking at 36 m s^{-1} , while broadening, from 2321:56 to 2322:44 UTC; and then contracts and reintensifies at 2322:59 UTC (Figs. 7, 10), approximately 470 m to the south of Reuters Road. Peak V_g exceeds 81 m s^{-1} as the subvortex, with $DX_{\text{max}} = 90\text{--}230 \text{ m}$, moves toward the north and then northwest, becoming nearly stationary over Reuters Road from 2323:35 to 2323:57 UTC, centered just to the east of the inferred starting position of the Samaras vehicle (and the location where the trunk contents were found). A distinct DRE surrounds the Samaras vehicle's location. The diameter of the debris ring increases in diameter from ~600 m to ~800 m from 2323:32 to 2324:13, an outward growth rate of $\sim 2\text{--}3 \text{ m s}^{-1}$. Subsequently, the vortex resumes its rapid eastward motion, crossing Radio Road, moving northeast then north with V_p as high as 79 m s^{-1} , and the DRE becomes more elliptical.

The last sighting of the Samaras vehicle's headlights, the location of the trunk contents, and the location where the vehicle was discovered are consistent with it being transported initially southward by strong northerly flow on the west side of the subvortex and then roughly eastward about the south side of the vortex as the vortex remained quasi stationary for about 20 s. The vehicle could have covered the approximately 600-m path from starting to ending location during the 20-s period that the subvortex was quasi stationary, if the vehicle was transported

at a plausible speed of about 30 m s^{-1} (recalling that $V_g > 70 \text{ m s}^{-1}$ on the south side of the subvortex during this period).

As the larger tornado/MVMC moved northeastward, two additional subvortices passed near these locations. One passed to the south of Reuters Road, likely causing strong easterly winds over the road, inconsistent with the eastward transport of the vehicle. The other grazed the road and may not have crossed over the intersection with Radio Road. The movement and evolution of the subvortex that was quasistationary over Reuters Road just before 2324 UTC is the most consistent with it transporting the vehicle.

A Weather Channel vehicle driving southward on US-81 penetrated into the tornado/MVMC in an attempt to traverse to the southern side of the tornadic region. It was impacted and damaged by the small central subvortex portion of the tornado/MVMC as the center of both the larger and smaller circulations crossed US-81, moving rapidly east-northeastward, with $V_p \sim 25 \text{ m s}^{-1}$ (Fig. 9). The high V_p likely contributed to its impacting the media vehicle. Westerly winds on the southern side of the central vortex exceeded 83 m s^{-1} at 120 m AGL and transported the vehicle to the east side of US-81, injuring the occupants.

OTHER INCIDENTS INVOLVING RESEARCH TEAMS INSIDE TORNADOES/MVMCS. While the fatalities and injuries caused by this tornado were unique, large tornadoes/MVMC such as this event have posed hazards to research

teams and those following them before. On 29 May 2004 a DOW team inadvertently was engulfed by the $\sim 2\text{-km } DX_{\max}$ circulation of a tornado/MVMC near Geary, Oklahoma. Visibility was near zero inside the circulation. Real-time radar imagery was employed to assist the DOW team in avoiding an interior subvortex translating in a complex path inside the main circulation. Despite this, winds of 87 m s^{-1} were documented at 12 m AGL near the DOW at the DX_{\max} of the larger circulation and the

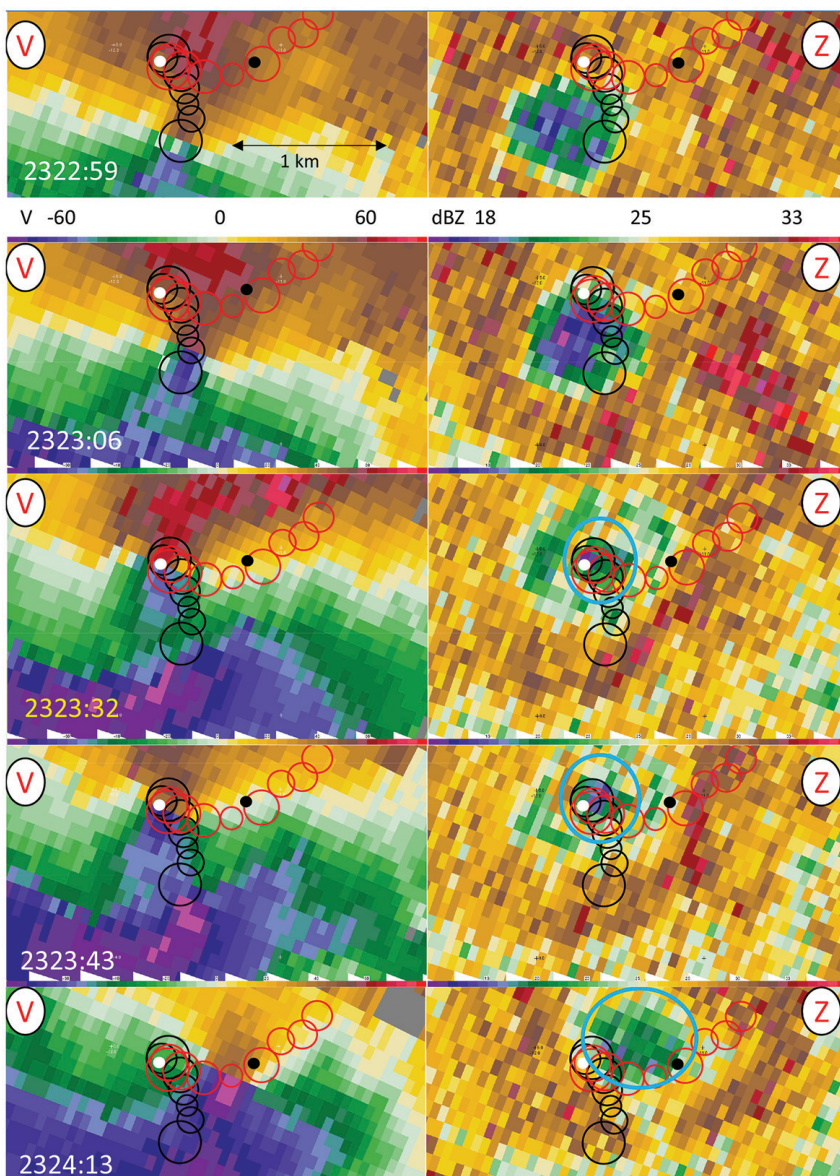


FIG. 10. (left) Doppler velocity and (right) reflectivity. DOW sweeps at selected times illustrating path of subvortex that impacted the Samaras research team. Red and black rings are schematic indications of region enclosing maximum winds. Times are in UTC. The blue ring in (right) annotates widening DRE. White/black dots are start/end location of vehicle. Beginning at $\sim 2323:32$ UTC, the vehicle was transported south and then east about the southern side of the subvortex.

DOW truck was damaged (WK13). The DOW crew would not have known to take actions to avoid the interior vortex without the real-time radar imagery the DOW provided.

On 5 May 2007, a media vehicle following a DOW was engulfed by a 2-km DX_{max} tornado/MVMC in Seward County, Kansas. Intense subvortices with $V_g > 96 \text{ m s}^{-1}$ revolved/spiraled about the

larger circulation. At least one of the subvortices itself contained sub-subvortices (WK13). These vortices passed close to, but not over, the media vehicle, which nevertheless suffered major damage. The driver was not injured.

CONCLUSIONS. The exceptionally large, complex, and intense El Reno tornado/MVMC of 31 May

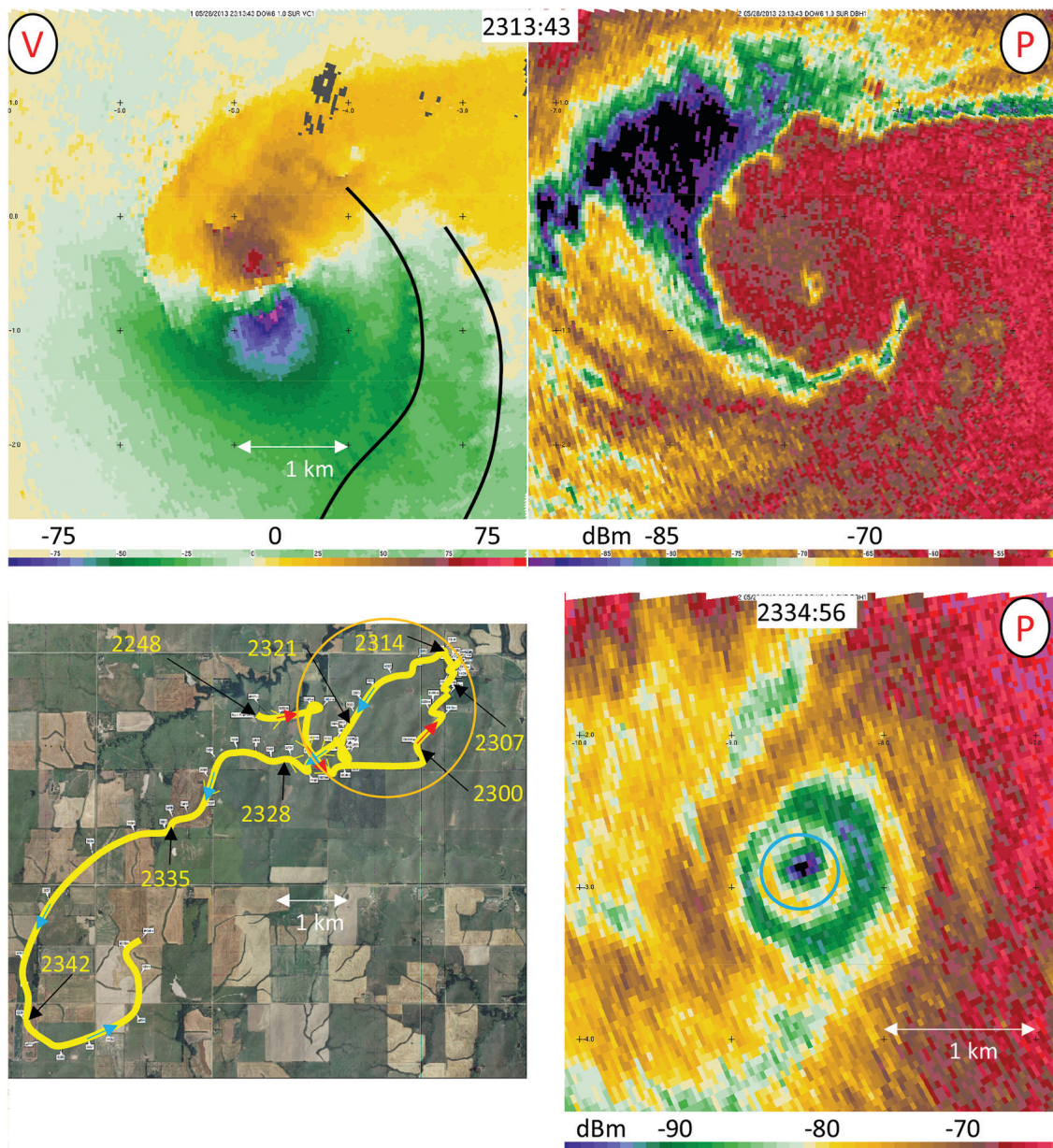


FIG. 11. (top left) Doppler velocity and (top right) received power in the Bennington, Kansas, tornado on 28 May 2013. Winds exceeded 118 m s^{-1} at 47 m AGL. (bottom left) Looping track of tornado from 2247 to 2347 UTC. Tornado formed before 2247 UTC, but DOW-based locations are less precise since the DOW was in motion. Tornado was nearly stationary from 2308 to 2313 UTC, moving less than 80 m over 300 s, and traced multiple loops during that and other periods, remaining within a 2.5-km-diameter circle (orange) for 2000 s. (bottom right) Discontinuous DRE as tornado passes over region with trees.

2013 killed eight people, including an experienced storm-chasing team that was likely impacted by an almost impossible to (visually) predict subvortex within the larger circulation. Both the Samaras and Weather Channel vehicles penetrated within the DX_{\max} (i.e., within the RMW) of the large tornado/MVMC circulation. Both penetrated the weak side of the MVMC/tornado, so they may have been unaware that they were inside. However, while the Samaras team was inside the tornado/MVMC, already in poor conditions and surrounded by even more intense winds, an interior subvortex, which transcribed a prolate cycloid path for the preceding ~ 200 s, intensified just 500 m to their south-southeast and moved north-northwestward, becoming nearly stationary just east of their vehicle. With only 30-s potential warning, possibly low visibility inside the RMW of the larger MVMC/tornado, and the anomalous and rapidly changing direction of movement of the subvortex, it is likely that no clear direction to safety was apparent. The Weather Channel team penetrated the larger tornado/MVMC, experiencing only moderately severe winds, but then was impacted by a very rapidly moving interior subvortex.

Though it was an interior subvortex that impacted both the Samaras and Weather Channel teams, some more simply structured singlet tornadoes exhibit highly anomalous tracks, adding to the hazard they pose to the public and those in pursuit. This tornado/MVMC became nearly stationary near Interstate 40 from 2329 to 2335 UTC, moving < 500 m during 300 s, a $V_p < 2$ m s^{-1} , and then abruptly resumed a more normal eastward motion. This type of motion is typical of maturing tornadoes revolving about mesocyclonic circulations. A striking example of unpredictable tornado path was exhibited by a violent tornado occurring near Bennington, Kansas, on 28 May 2013. The tornado persisted for over 4000 s; near-surface Doppler winds reached 118 m s^{-1} , a double gust front structure (Wurman et al. 2007a; Marquis et al. 2008; Kosiba et al. 2013) was observed, and a discontinuous DRE developed as the tornado crossed over a region with trees (Fig. 11). The forward speed of the tornado typically was quite slow, < 0.3 m s^{-1} over 300 s, and the track looped back on itself. Observers “behind” the tornado remained at considerable risk.

What role can technology play in enhancing the safety of missions near tornadoes? Research teams who deploy in situ tornado pods during the Radar Observations of Tornadoes and Thunderstorms Experiment (ROTATE; Wurman 2008) operate under the safety umbrella provided by real-time DOW mapping of tornado winds updating every

7 s, which provides detailed information concerning tornado intensity, size, multiple-vortex structure, and changing path. DOW real-time scanning was critical to team safety when the DOW was inside the Geary, Oklahoma, tornado/MVMC, allowing the DOW to avoid an optically invisible interior subvortex. The ROTATE science team navigated outside the DX_{\max} of the after-dark and invisible tornado/MVMC in Seward, Kansas, using DOW-provided information. ROTATE tornado pod deployment missions are aborted if real-time DOW radar coverage is lost. Critically, the ROTATE team aborted their attempt to deploy tornado pods in the El Reno tornado when real-time DOW data revealed a violent, complex, and large circulation with an additional anticyclonic tornado to the south and aborted their mission on the Bennington, Kansas, tornado because of a lack of track predictability.

A few storm chasers have employed armored vehicles to provide safety inside DX_{\max} [e.g., the Tornado Intercept Vehicle (TIV); Wurman et al. 2007b, 2013]. These likely provide substantial added protection, but none are engineered rigorously against the most intense winds or debris hazards. DOWs have armored cabins and low centers of gravity providing protection against moderate intensity winds and debris typical of some tornadoes and most hurricanes, but tornado pod deployment trucks are not armored. The Samaras team’s Chevy Cobalt was not especially heavy or armored, likely adding to its vulnerability once the team penetrated the region inside DX_{\max} of the tornado/MVMC.

Chasing tornadoes can appear to be a low-risk activity based on the rarity of injuries and fatalities. However, without access to real-time mobile radar data, storm chasers, particularly those attempting to deploy instrumentation inside tornadoes or film especially close to tornadoes, may inadvertently penetrate the RMW of large tornadoes/MVMCs and find themselves particularly vulnerable to intense winds contained in interior subvortices such as those documented in Geary (2004), Seward (2007), and El Reno (2013). The fatal and nonfatal incidents documented here should provide a cautionary note to those pursuing activities near tornadoes, with particular focus on the hazards of penetrating within the RMW of large tornadoes/MVMCs.

ACKNOWLEDGMENTS. This analysis and the DOWs are supported by National Science Foundation Grants AGS-121132 and AGS-080401. The Samaras/TWISTEX mission was funded independently. Thanks to Dan Robinson for providing video documentation and to Warren Faidley

and Jimmy Deguara for providing photographs of the Weather Channel and Samaras vehicles. Thanks to the ROTATE crew for collecting data in a very challenging environment. Thanks to Rachel Humphrey for assisting with the manuscript.

REFERENCES

- Alexander, C. R., and J. Wurman, 2008: Updated mobile radar climatology of supercell tornado structures and dynamics, *Proc. 24th Conf. on Severe Local Storms*, Savannah, GA, Amer. Meteor. Soc., 19.4. [Available online at <http://ams.confex.com/ams/pdfpapers/141821.pdf>.]
- Bluestein, H. B., 1999: A history of storm-intercept field programs. *Wea. Forecasting*, **14**, 558–577.
- , and A. Bedard, 1982: Surface meteorological observations in severe thunderstorms: Field measurements and design detail of TOTO. *Proc. 12th Conf. on Severe Local Storms*, San Antonio, TX, Amer. Meteor. Soc., 383–395.
- , and A. L. Pazmany, 2000: Observations of tornadoes and other convective phenomena with a mobile, 3-mm wavelength, Doppler radar: The spring 1999 field experiment. *Bull. Amer. Meteor. Soc.*, **81**, 2939–2351.
- , S. G. Gaddy, D. C. Dowell, A. L. Pazmany, J. C. Galloway, R. E. McIntosh, and H. Stein, 1997: Doppler radar observations of substorm-scale vortices in a supercell. *Mon. Wea. Rev.*, **125**, 1046–1059.
- , C. C. Weiss, and A. L. Pazmany, 2003: Mobile Doppler radar observations of a tornado in a supercell near Bassett, Nebraska, on 5 June 1999. Part I: Tornadogenesis. *Mon. Wea. Rev.*, **131**, 2954–2967.
- , —, and —, 2004: The vertical structure of a tornado near Happy, Texas, on 5 May 2002: High-resolution, mobile, W-band, Doppler radar observations. *Mon. Wea. Rev.*, **132**, 2325–2337.
- , M. M. French, R. L. Tanamachi, S. Frasier, K. Hardwick, F. Junyent, and A. L. Pazmany, 2007: Close-range observations of tornadoes in supercells made with a dual-polarization, X-band, mobile Doppler radar. *Mon. Wea. Rev.*, **135**, 1522–1543.
- Brock, F. V., G. Lesins, and R. Walko, 1987: Measurement of pressure and air temperature near severe thunderstorms: An inexpensive and portable instrument. *Extended abstracts, Sixth Symp. on Meteorological Observations and Instrumentation*, New Orleans, LA, Amer. Meteor. Soc., 320–323.
- Dowell, D. C., C. R. Alexander, J. M. Wurman, and L. J. Wicker, 2005: Centrifuging of hydrometeors and debris in tornadoes: Radar-reflectivity patterns and wind-measurement errors. *Mon. Wea. Rev.*, **133**, 1501–1524.
- Hastings, R. M., Y. P. Richardson, P. Markowski, J. Wurman, and C. C. Weiss, 2012a: Mergers in supercell environments. Part I: Conceptual models of mechanisms governing merger outcomes. Preprints, *26th Conf. on Severe Local Storms*, Nashville, TN, Amer. Meteor. Soc., 11B.6. [Available online at <https://ams.confex.com/ams/26SLS/webprogram/Paper212519.html>.]
- , —, and —, 2012b: Mergers in supercell environments. Part II: Tornadogenesis potential during merger as evaluated by changes in the near-surface low-level mesocyclone. Preprints, *26th Conf. on Severe Local Storms*, Nashville, TN, Amer. Meteor. Soc., P143. [Available online at <https://ams.confex.com/ams/26SLS/webprogram/Paper212524.html>.]
- Karstens, C. D., T. M. Samaras, B. D. Lee, W. A. Gallus Jr., and C. A. Finley, 2010: Near-ground pressure and wind measurements in tornadoes. *Mon. Wea. Rev.*, **138**, 2570–2588.
- Kosiba, K., and J. Wurman, 2010: The three-dimensional axisymmetric wind field structure of the Spencer, South Dakota, 1998 tornado. *J. Atmos. Sci.*, **67**, 3074–3083.
- , and —, 2013: The three-dimensional structure and evolution of a tornado boundary layer. *Mon. Wea. Rev.*, **28**, 1552–1561.
- , R. J. Trapp, and J. Wurman, 2008: An analysis of the axisymmetric three-dimensional low level wind field in a tornado using mobile radar observations. *Geophys. Res. Lett.*, **35**, L05805, doi:10.1029/2007GL031851.
- , J. Wurman, Y. Richardson, P. Markowski, P. Robinson, and J. Marquis, 2013: Genesis of the Goshen County, Wyoming, tornado on 5 June 2009 during VORTEX2. *Mon. Wea. Rev.*, **141**, 1157–1181.
- Kumijan, M. R., 2011: Precipitation properties of supercell hook echoes. *E-J. Severe Storms Meteor.*, **6**, 1–21.
- Lee, B. D., C. A. Finley, and T. M. Samaras, 2011: Surface analysis near and within the Tipton, Kansas, tornado on 29 May 2008. *Mon. Wea. Rev.*, **139**, 370–386.
- Lee, J. J., T. M. Samaras, and C. R. Young, 2004: Pressure measurements at the ground in an F-4 tornado. Preprints, *22nd Conf. on Severe Local Storms*, Hyannis, MA, Amer. Meteor. Soc., 15.3.
- Lee, W.-C., and J. Wurman, 2005: The diagnosed structure of the Mulhall tornado. *J. Atmos. Sci.*, **62**, 2373–2393.
- Marquis, J. N., Y. P. Richardson, J. M. Wurman, and P. M. Markowski, 2008: Single- and dual-Doppler analysis of a tornadic vortex and surrounding storm scale flow in the Crowell, TX, supercell of 30 April 2000. *Mon. Wea. Rev.*, **136**, 5017–5043.

- Ryzhkov, A. V., T. J. Schuur, D. W. Burgess, and D. S. Zrnic, 2005: Polarimetric tornado detection. *J. Appl. Meteor.*, **44**, 557–570.
- Samaras, T. M., 2004: A historical perspective of in-situ observations within tornado cores. Preprints, *22nd Conf. on Severe Local Storms*, Hyannis, MA, Amer. Meteor. Soc., P11.4.
- Tanamachi, R. L., H. B. Bluestein, W.-C. Lee, M. Bell, and A. Pazmany, 2007: Ground-based velocity track display (GBVTD) analysis of W-band Doppler radar data in a tornado near Stockton, Kansas, on 15 May 1999. *Mon. Wea. Rev.*, **135**, 783–800.
- Tatom, F. B., and K. R. Knupp, 1995: Tornado detection based on seismic signal. *J. Appl. Meteor.*, **34**, 572.
- van Doren, C., 1938: *Benjamin Franklin*. Viking Press, 845 pp.
- Wakimoto, R. M., P. Stauffer, W.-C. Lee, N. T. Atkins, and J. Wurman, 2012: Finescale structure of the LaGrange, Wyoming, tornado during VORTEX2: GBVTD and photogrammetric analyses. *Mon. Wea. Rev.*, **140**, 3397–3418.
- Winn, W. P., S. J. Hunyady, and G. D. Aulich, 1999: Pressure at the ground in a large tornado. *J. Geophys. Res.*, **104**, 22067–22082.
- Wurman, J., 2002: The multiple-vortex structure of a tornado. *Wea. Forecasting*, **17**, 473–505.
- , 2008: Preliminary results and report of the ROTATE-2008 radar/in-situ/mobile mesonet experiment. Preprints, *24th Conf. on Severe Local Storms*, Savannah, GA, Amer. Meteor. Soc., 5.4.
- , and S. Gill, 2000: Finescale radar observations of the Dimmitt, Texas (2 June 1995), tornado. *Mon. Wea. Rev.*, **128**, 2135–2164.
- , and T. Samaras, 2004: Comparison of in-situ pressure and DOW Doppler winds in a tornado and RHI vertical slices through 4 tornadoes during 1996–2004. Preprints, *22nd Conf. on Severe Local Storms*, Hyannis, MA, Amer. Meteor. Soc., 15.4. [Available online at <http://ams.confex.com/ams/pdfpapers/82352.pdf>.]
- , and K. A. Kosiba, 2008: DOW observations of multiple vortex structure in several tornadoes. Preprints, *24th Conf. on Severe Local Storms*, Savannah, GA, Amer. Meteor. Soc., P3.20. [Available online at <http://ams.confex.com/ams/pdfpapers/142194.pdf>.]
- , and —, 2013: Finescale radar observations of tornado and mesocyclone structures. *Wea. Forecasting*, **28**, 1157–1174.
- , J. Straka, and E. Rasmussen, 1996: Fine Scale Doppler Radar Observation of Tornadoes. *Science*, **272**, 1774–1777.
- , J. Straka, E. Rasmussen, M. Randall, A. Zahrai, 1997: Design and Deployment of a Portable, Pencil-Beam, Pulsed Doppler Radar. *J. Atmos. Oceanic Technol.*, **14**, 1502–1512.
- , Y. Richardson, C. Alexander, S. Weygandt, and P. F. Zhang, 2007a: Dual-Doppler and single-Doppler analysis of a tornadic storm undergoing mergers and repeated tornadogenesis. *Mon. Wea. Rev.*, **135**, 736–758.
- , P. Robinson, C. Alexander, and Y. Richardson, 2007b: Low-level winds in tornadoes and potential catastrophic tornado impacts in urban areas. *Bull. Amer. Meteor. Soc.*, **88**, 31–46.
- , D. Dowell, Y. Richardson, P. Markowski, E. Rasmussen, D. Burgess, L. Wicker, and H. B. Bluestein, 2012: The second Verification of the Origins of Rotation in Tornadoes Experiment: VORTEX2. *Bull. Amer. Meteor. Soc.*, **93**, 1147–1170.
- , K. A. Kosiba, and P. Robinson, 2013: In situ, Doppler radar, and video observations of the interior structure of a tornado and the wind–damage relationship. *Bull. Amer. Meteor. Soc.*, **94**, 835–846.

AMS titles now available as eBooks at **springer.com**

AMS BOOKS

RESEARCH APPLICATIONS HISTORY

www.ametsoc.org/amsbookstore



Scan to see
AMS eBook titles
at springer.com



AMERICAN METEOROLOGICAL SOCIETY